Matter

CellPress

Article

Bioinspired super-strong aqueous synthetic tissue adhesives

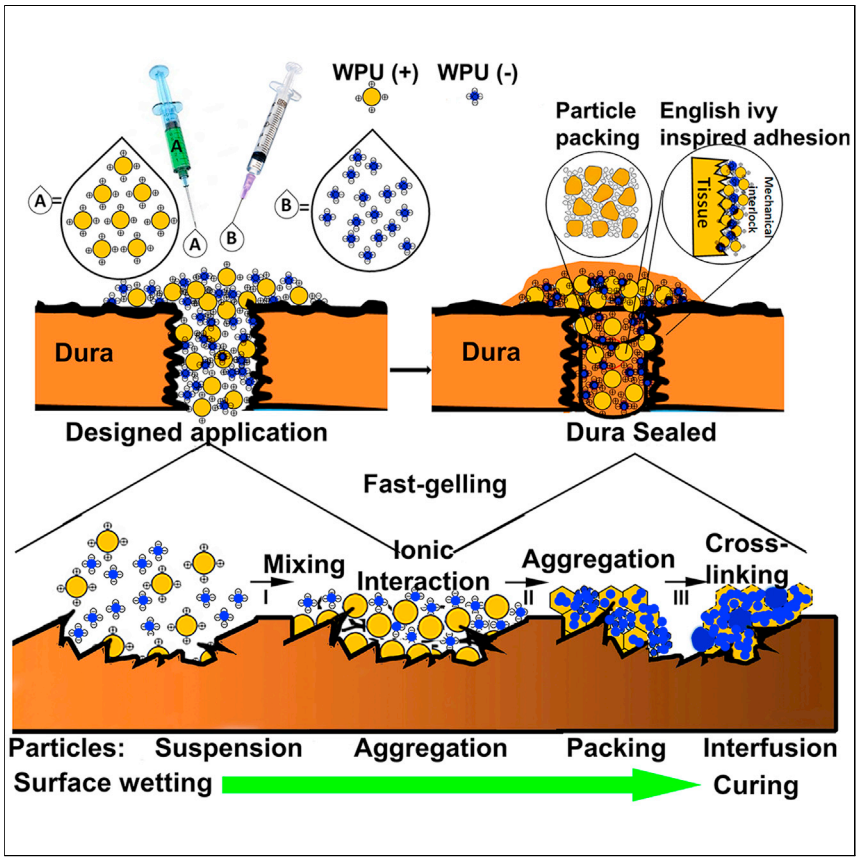

Existing tissue adhesives and sealants are far from satisfactory when applied on wet and dynamic tissues. We report a strategy for designing a biodegradable, fast-gelling, super strong, elastic, and aqueous glue (B-Seal) for surgical uses inspired by an English ivy adhesion strategy and a cement particle packing theory. B-Seal is composed of biodegradable polyurethane nanodispersions with mismatched particle sizes and counterions in its A-B formulation. The design of B-Seal represents a new direction of designing the next-generation wet tissue adhesives for surgeries.

Qing Li, Wei Song, Jinghui Li, ..., Elias B. Rizk, Di Lu, Chao Liu

erizk@pennstatehealth.psu.edu (E.B.R.)
ludi20040609@126.com (D.L.)
ch.liu@aleobme.com (C.L.)

Highlights

B-Seal is a fast-gelling, super strong, elastic, and aqueous adhesive sealant

B-Seal is composed of waterborne biodegradable polyurethane nanodispersions

B-Seal is designed under a plant adhesion and cement particle packing theory

B-Seal can successfully seal and repair leaky dura in a pig craniotomy model

1 **Discovery**
A new material or phenomena

Li et al., Matter 5, 933–956
March 2, 2022
https://doi.org/10.1016/j.matt.2021.12.018

Matter

CellPress

Article

Bioinspired super-strong aqueous synthetic tissue adhesives

Qing Li,[1,6] Wei Song,[2,6] Jinghui Li,[3,6] Chuying Ma,[2,6] Xinxiang Zhao,[4] Jianlin Jiao,[1] Oliver Mrowczynski,[5] Becky S. Webb,[5] Elias B. Rizk,[5,*] Di Lu,[1,*] and Chao Liu[2,7,*]

SUMMARY

Existing tissue adhesives and sealants are far from satisfactory when applied on wet and dynamic tissues. Herein, we report a strategy for designing a biodegradable, super-strong aqueous glue (B-Seal) for surgical uses, inspired by an English ivy adhesion strategy and a cement particle packing theory. B-Seal is a fast-gelling, super strong, and elastic adhesive sealant composed of injectable waterborne biodegradable polyurethane (WPU) nanodispersions with mismatched particle sizes and counterions in its A-B formulation. B-Seal showed 24-fold greater burst pressure than DuraSeal, 138-fold greater T-pull adhesive strength than fibrin glue, and 16-fold greater lap shear strength than fibrin glue. *In vivo* evaluation on a rat cerebrospinal fluid (CSF) rhinorrhea model and a porcine craniotomy model validated the safety and efficacy of B-Seal for effective CSF leak prevention and dura repair. The plant-inspired adhesion strategy combined with particle packing theory represents a new direction for designing the next-generation wet tissue adhesives for surgeries.

INTRODUCTION

Bioadhesives, including tissue adhesives and sealants, have gained increasing popularity as an alternative to sutures and staples to achieve tissue closure, hemostasis, and medical device fixation in recent years due to their ease of use, airtight or watertight sealing, and minimal tissue damage.[1] However, commercial bioadhesives are far from satisfactory when applied on wet and dynamic tissue surfaces, such as lung, heart muscle, gastrointestinal (GI) tissue, dural tissue, amniotic sac, and so on.[2] For example, cyanoacrylate (CA) glue is commonly used due to its fast curing and strong adhesion, but its cytotoxic and rigid nature limits the applications mostly for topical use.[3] Fibrin glues, such as Tisseel and Evicel,[4] only slowly and weakly adhere to tissue. Similar to fibrin glues, poly(ethylene glycol) (PEG)-based adhesives, such as DuraSeal, form fragile matrices that are vulnerable to debonding due to poor adhesive and cohesive strengths and their rapid swelling and degradation. Thus, it remains a significant challenge to develop a bioadhesive that can function both as a tissue adhesive and a sealant on wet and dynamic tissues and requires well-balanced curing times, adhesive and cohesive strengths, elasticity, and degradation rates.

The last decade has witnessed transformative advances in developing wet tissue adhesives, especially hydrogel-based adhesives made from proteins, peptides, polysaccharides, and synthetic polymers.[4–8] The underlying adhesion mechanisms are attributed to either non-covalent interactions, such as hydrogen bonding, ionic bonding, host-guest interactions, and mechanical interlocking, or covalent

Progress and potential

It remains a significant challenge to develop a bioadhesive that can function as both a tissue adhesive and a sealant on wet and dynamic tissues such as lung tissue, heart muscle, gastrointestinal (GI) tissue, dural tissue, amniotic sac, and so on. We report a strategy for designing a biodegradable, super-strong aqueous synthetic glue (B-Seal) for surgical uses inspired by an English ivy adhesion strategy and a cement particle packing theory without using any toxic chemical cross-linking. B-Seal offers advantages over the existing tissue adhesives and sealants, including its fast tissue adhesion, super-strong wet tissue adhesion strengths, tenacity and flexibility, long shelf life, and excellent *in vivo* safety and efficacy for CSF leak prevention and dura repair. The design strategy of B-Seal represents a new direction for designing the next generation of tissue adhesives and sealants to address the challenging problems related to leak prevention and tissue regeneration in various surgeries.

interactions through various chemical cross-linking reactions between cross-linkable groups, such as azide/alkyne, thiol/ene, amine/yne, or amine/N-hydrosuccinimide (NHS), or their combinations.[9–11] However, hydrogel-based adhesives are usually weak in their wet adhesion strengths (<50 kPa) partly due to (1) the hydration layers at the tissue surfaces not only significantly weakening the non-covalent interactions but also hampering the covalent cross-linking reactions; (2) the lack of energy dissipative capacity for soft hydrogels;[2,12] and (3) the mismatched cohesive strengths between the soft hydrogels and tissues, thus resulting in the premature failure of the hydrogels themselves.

More recently, significant attention has been dedicated to developing nature-inspired wet tissue adhesives. Inspirations were drawn from adhesions of animals, such as mussels, barnacles, salamander, gecko, and spiders, that are capable of fast-forming strong adhesion in a wet environment. Their secreted adhesive proteins can remove interfacial water at the contact surface to form strong bonding via both covalent and non-covalent interactions.[13–19] Wet tissue adhesives usually take a tape form or a liquid form. A promising dry double-sided tape (DST) has been recently developed using a combination of a biopolymer (gelatin or chitosan) and NHS ester-modified cross-linked poly(acrylic acid) (PAAc-NHS ester).[20] DST exhibits strong adhesion (shear strength >120 kPa) by quickly absorbing interfacial water through DST swelling and rapid reaction (within a few minutes) between NHS and primary amines on tissues. Although promising, the adhesive tape form may limit how the DST can be applied in complex medical conditions. Many synthetic bioadhesives are designed as injectable materials by mimicking the animal adhesion mechanisms, such as catechol-associated mussel adhesions. These adhesives are usually dissolved in water and then cross-linked into hydrogels and bonded to wet tissues.[21–24] However, the incredible feats that animals display for wet adhesion can be barely replicated by the current synthetic wet tissue adhesive materials, likely due to the hydrophilic nature of the synthesized water-soluble materials that are unable to remove the interfacial water effectively. Developing biomimetic synthetic wet tissue adhesives is still a significant technical barrier to overcome.

Plant-derived adhesion mechanisms have also attracted significant attention in recent years. For example, English ivy (hedera helix) is known for its ability to climb surfaces and impose adhesive forces strong enough to tear bricks from walls and wear away building facades. The plant secretes nanospheric glycoprotein particles that intercalate and aggregate on a target surface. These nanoparticles form a penetrating film that is further strengthened via cross-linking by calcium, thus enabling mechanical interlocking between the roots of English ivy and the surface to which it clings. Inspired by English ivy adhesion, arabinogalactan proteins (AGPs)-rich nanoparticles were shown to form a mechanical interlocking film on the rough surfaces in combination with calcium ions, thus forming high strength adhesion.[25] However, such promising adhesion strategies have not been translated into effective wet tissue adhesive design.

Based on the culmination of current understanding of tissue adhesion mechanisms, we report a design of fast-acting bioinspired super-strong aqueous glues (B-Seal) for surgical uses, exemplified for dural repair and regeneration. B-Seal is a plant-inspired A-B formulation composed of injectable biodegradable waterborne polyurethane (WPU) nanodispersions with counterions in the A and B components, respectively. The unique features of B-Seal are multifaceted: (1) B-Seal represents the first aqueous synthetic tissue adhesive adopting the unique adhesion strategy

[1]Yunnan Key Laboratory of Stem Cell and Regenerative Medicine, Science and Technology Achievement Incubation Center, Kunming Medical University, Kunming 650500, China

[2]Aleo BME, State College, PA 16803, USA

[3]Department of Neurosurgery, First Affiliated Hospital, Kunming Medical University, Kunming, 650031, China

[4]Department of Radiology, Second Affiliated Hospital, Kunming Medical University, Kunming, 650032, China

[5]Department of Neurosurgery, Milton S. Hershey Medical Center, The Pennsylvania State University, Hershey, PA 17033, USA

[6]These authors contributed equally

[7]Lead contact

*Correspondence: erizk@pennstatehealth.psu.edu (E.B.R.), ludi20040609@126.com (D.L.), ch.liu@aleobme.com (C.L.)

https://doi.org/10.1016/j.matt.2021.12.018

of English ivy for tissue adhesion without using toxic chemical cross-linking and a cement particle packing theory for enhanced packing density and mechanical strengths;[26] (2) B-Seal is a fast-gelling (<10 s), super-strong (equivalent to Dermabond), and elastic adhesive sealant that exhibits a swelling ratio below 10%, eliminating the swelling problems that occur in the use of PEG hydrogel-based adhesives, such as DuraSeal; (3) the high solid content of B-Seal (up to 50 wt %) makes it ideal to serve as both an adhesive sealant and a scaffold for tissue repair; (4) B-Seal presents tunable degradation to sustain a long-term seal and match the tissue healing rate, eliminating the problems found in using fibrin glue and DuraSeal that are notoriously known to be rapidly degraded in the wound; and (5) the fully synthetic B-Seal is easy to manufacture in a cost-effective manner. *In vivo* evaluation on a rat cerebrospinal fluid (CSF) rhinorrhea model and a porcine craniotomy model validated the safety and efficacy of B-Seal for effective CSF leak prevention and dura repair.

RESULTS

B-Seal adhesion mechanisms

The B-Seal is an A-B formulation, in which component A is composed of positively charged WPU nanoparticle dispersion (WPU [+]) and component B is composed of negatively charged WPU nanoparticle dispersion (WPU [−]) (Figure 1A). B-Seal adhesion mechanism is a unique combination of an English ivy adhesion mechanism, through which WPU (+) and WPU (−) nanoparticles penetrate and permeate onto tissue surfaces and then ionically cross-link to form a strong mechanical interlocking at the adhesive/tissue interface, and particle packing theory, through which particle size mismatch plays a significant role in enhancing particle packing and interfusion for improving adhesive and cohesive strengths of the adhesive. Figures 1A and 1B depict the proposed mechanism of B-Seal for tissue adhesion. The mixing of A and B will result in rapid gelation within 10 s (Figure S1) due to ionic cross-linking, a cross-linking mechanism for adhesion simulating that of English ivy, in which calcium acts as an ionic cross-linker instead to cross-link glycoprotein nanoparticles.[25] The permeation and penetration of nanoparticles on damaged tissue surfaces and the gelation through nanoparticle packing, irreversible particle interfusion, and ionic cross-linking of components A and B accelerate the coalescence of WPU nanoparticles on the tissue surface to form a mechanically interlocked interface. Furthermore, the mismatched particle sizes of WPU (+) and WPU (−) provide a highly packed structure simulating particle packing in the cement industry (Figure 1B), which further increases the density and mechanical strength of B-Seal.

B-Seal synthesis and characterization

Biodegradable WPUs were synthesized via two-step reactions (a prepolymer step and a chain extension step) using ε-polycaprolactone diol (PCL-diol) and aliphatic diisocyanate (di-NCO), isophorone diisocyanate (IPDI) as the main reactants; stannous octoate ($Sn(Oct)_2$) as a catalyst; 1,4-butanediol (BDO) and ethylenediamine (EDA) as the neutral chain extender (NCE); and dimethylol propionic acid (DMPA, for WPU [−]) or N-methyl diethanolamine (MDEA, for WPU [+]) as the ionic chain extenders (ICEs). We synthesized WPU (+)/(−) nanodispersions with a range of particle sizes by controlling the NCO/diol/ICE reaction times. For WPU (+) particles, the sizes are defined as extra-large (XL; >300 nm), large (L; 160–300 nm), medium (M; 130–160 nm), medium-small (MS; 90–130 nm), and small (S; <90 nm). For WPU (−) particles, the sizes are defined as XL (>300 nm), L (150–300 nm), M (120–150 nm), MS (90–120 nm), S (50–90 nm), and extra-small (XS; <50 nm). B-Seal was formulated by mixing WPU (+) with a chosen particle size in the range of 70–350 nm (Figure S2A) and WPU (−) with a chosen particle size in the range of 45–350 nm (Figure S2B) at a

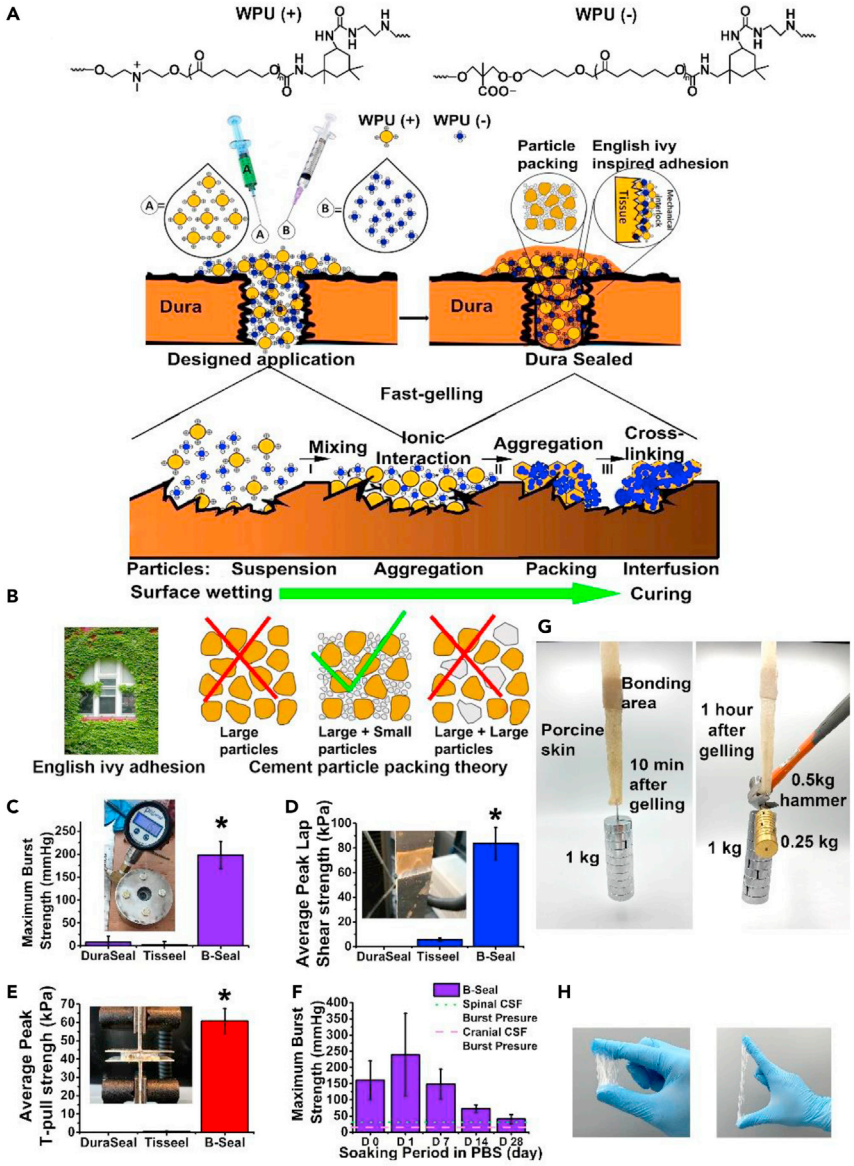

Figure 1. Proposed mechanism of B-Seal and mechanical comparison with commercial products

(A and B) Schematic representation of the adhesion mechanism of nature-inspired (English ivy adhesion + cement particle packing theory) B-Seal that is composed of WPU (+) (yellow) nanodispersion and WPU (–) (blue) nanodispersion.

(C) The burst strengths of Tisseel (fibrin glue), DuraSeal, and B-Seal.

(D) The lap shear strengths of Tisseel (fibrin glue), DuraSeal, and B-Seal.

(E) The T-pull adhesive strengths of Tisseel (fibrin glue), DuraSeal, and B-Seal.

(F) The burst strengths of B-Seal soaked in pH 7.4 PBS at 37°C over time (n = 5, *p < 0.05); dotted lines represent the typical spinal and cranial CSF pressures.

(G and H) Demonstration of elasticity and strong adhesion of B-Seal on (G) porcine skin and (H) nitrile gloves

1:1 volume ratio. The nanoparticles in B-Seal have a zeta potential in the range of $\pm 30 \sim \pm 60$ mV, indicating a stable particle dispersion,[27] as shown in (Figures S2C and S2D). The B-Seal used in the subsequent studies is referred to XL WPU (+) and XS WPU (–), unless otherwise specified.

Figures S3A–S3C show the attenuated total reflectance (ATR)-Fourier transform infrared spectroscopy (FTIR) spectra of films composed of single WPU and B-Seal films composed of mixed WPU (+)/(−) with mismatched particle sizes. Absorbance from the urethane bonds was observed in the form of a shoulder peak at 3350 cm^{-1} on all films. There are no peaks at 2267 cm^{-1} observed, suggesting that the isocyanate groups had been completed consumed in all the WPU syntheses. The peaks at 1675–1750 cm^{-1} were assigned to the carbonyl groups (C=O) in urethane bonds, and the peaks at 1625–1675 cm^{-1} were assigned to carbonyl groups in urea bonds. More specifically, the peaks of carbonyl groups were divided into 5 regions according to the different forms of hydrogen bonding:[28–30] free urethane, H-bonded urethane, free urea, monodentate urea, and bidentate urea, as highlighted in Figures S3B and S3C. The chemical compositions of WPU (+)/(−) were also confirmed by ^{1}H-NMR (Figures S3D–S3E). The peaks at 4.20 and 3.98 ppm were assigned to -C$\underline{H}_2$-O- from PCL-diol. The small broad peak at around 3.57 ppm was partially contributed by the protons from -C$\underline{H}_2$- linked to the urethane bonds (-NHC(O)O-C$\underline{H}_2$-) whereas the peak around 2.99 ppm was assigned to the -C$\underline{H}_2$- linked to the urea bonds (-NHC(O)NH-C$\underline{H}_2$-).To demonstrate the degradability of B-Seal, B-Seal was incubated in PBS, 20 wt % hydrogen peroxide (H_2O_2) supplemented with 0.1 M cobalt chloride ($CoCl_2$) and PBS containing 1 U/mL cholesterol esterase (CE); B-Seal showed almost no degradation in PBS but significantly accelerated degradation (25%–30% weight loss) in oxidative and enzymatic environments within 16 weeks (Figure S3F). Nonetheless, the *in vitro* degradation of B-Seal is slow.

Mechanical properties of B-Seal

Burst pressure, lap shear, and T-pull strengths are key parameters for cohesive and adhesive properties of tissue adhesives. The above mechanical properties of selected B-Seal formulations (XL/XS and M/S), Tisseel (fibrin glue), and DuraSeal (a commercial NHS functionalized PEG [PEG-NHS]-based adhesive) on wet porcine tissues were evaluated under the same test conditions according to respective American Society for Testing and Materials (ASTM) protocols. B-Seal showed 24-fold greater burst pressure (198.33 ± 29.64 mm Hg; 26.44 ± 3.95 kPa) than DuraSeal (8.29 ± 13.11 mm Hg; 1.1 ± 1.75 kPa) whereas Tisseel failed to record a value during the test after the wet conditioning (ASTM F2392-04, Figure 1C). B-Seal also showed 138-fold greater T-pull adhesive strength (60.67 ± 6.94 kPa) than fibrin glue (0.44 ± 0.24 kPa) (ASTM 2258, Figure 1D) and 16-fold greater lap shear strength (83.67 ± 12.92 kPa) than fibrin glue (5.47 ± 1.47 kPa) (ASTM F2205, Figure 1E) whereas DuraSeal failed during both tests after wet conditioning due to extremely weak adhesion. To determine the adhesion/sealing properties over time for applications, such as CSF leak repair, an approximately 1-mm-thick B-Seal was applied on a porcine intestine casing and incubated at 37°C in pH 7.4 PBS for up to 4 weeks to simulate the extreme wet conditions before it was mounted on the test fixture for burst pressure tests. Figure 1F shows that B-Seal continued setting and reached an impressive maximum burst pressure of averaging 230 mm Hg (30.66 kPa) 1 day after soaking in PBS. Throughout the 4-week soaking in PBS, the sealant continued to maintain burst pressures well above the physiological levels that may be experienced in the spine, demonstrating that B-Seal can withstand representative spikes (up to 45 mm Hg) in CSF pressure for at least 4 weeks in such an extreme soaking condition. Therefore, B-Seal is well poised for wet tissue adhesion applications. Figure 1G shows the B-Seal-bonded porcine skins withstand heavy loads of 1 and 1.3 kg after being gelled for 10 min and 1 h, respectively. Interestingly, B-Seal demonstrated a favorable tenacity (adhesive and elastic), as shown in Figure 1H. The B-Seal firmly adhered to the nitrile gloves and underwent large deformation without failure.

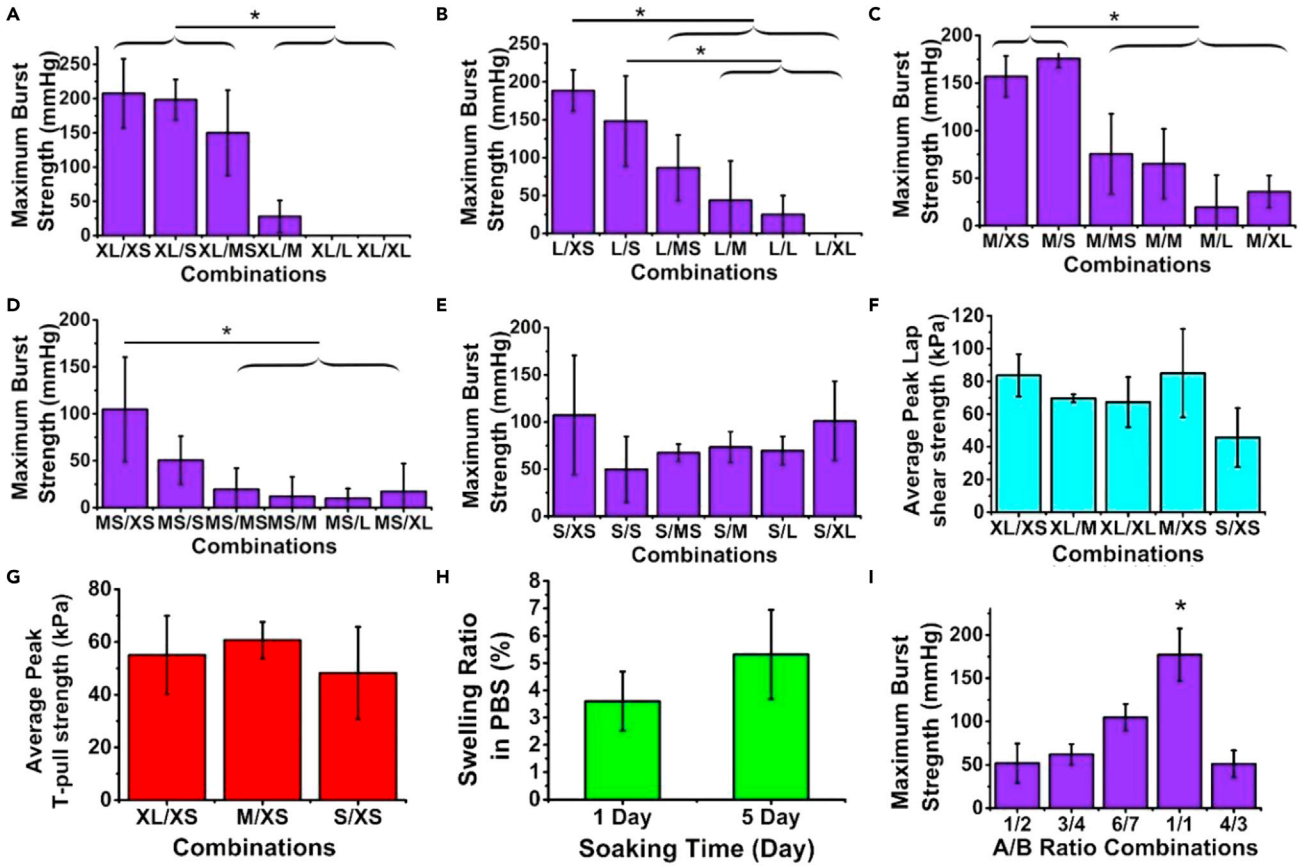

Figure 2. Characterization of lap shear strengths, T-pull strengths, burst strengths, and swelling of B-Seal formulations with various size pairs of WPU (+)/WPU (−)

(A–E) The burst strengths of B-Seal at various particle size pairs (n = 6, *p < 0.05).

(F) The lap shear strength of B-Seal at various particle size pairs (n = 6).

(G) The T-pull strength of B-Seal at various particle size pairs (n = 6).

(H) The swelling ratio of B-Seal film soaked in 37°C PBS for 1 and 5 days (n = 3).

(I) The burst strengths of B-Seal at A-B volume ratios of 1:2, 3:4, 6:7, 1:1, and 4:3 (n = 6). *p < 0.05. For WPU (+) particles, the sizes are defined as extra-large (XL; >300 nm), large (L; 160–300 nm), medium (M; 130–160 nm), medium-small (MS; 90–130 nm), and small (S; <90 nm). For WPU (−) particles, the sizes are defined as extra-large (XL; >300 nm), large (L; 150–300 nm), medium (M; 120–150 nm), medium-small (MS; 90–120 nm), small (S; 50–90 nm), and extra-small (XS; <50 nm).

Enhancing B-Seal adhesion through particle size mismatches

Burst pressure reflects the adhesive strength and cohesive strength; thus, it is an excellent measure of characterizing the performance of tissue adhesive sealants. Surprisingly, we found that the size mismatch between component A and component B in the B-Seal formulation plays a significant role in determining the burst pressure of the B-Seal, as shown in Figures 2A–2E. Burst pressure was measured on porcine intestine casings sealed by B-Seal. Among all the size pairs investigated, WPU (+) (XL, L, MS, and S) mixed with WPU (−) XS ranked the highest strength (Figures 2A–2E), whereas WPU (+) M with WPU (−) XS ranked the second highest. In general, the larger size differences between WPU (+) and WPU (−) yield higher burst pressure. However, when both particles are relatively small, even the size difference is not a large difference, such as S/XS; as shown in Figure 2E, B-Seal still showed significant burst pressure (around 100 mm Hg/13.33 kPa). Most of the B-Seal particle combinations exceeded the maximum burst pressure in cranial and spinal CSF (up to 45 mm Hg).

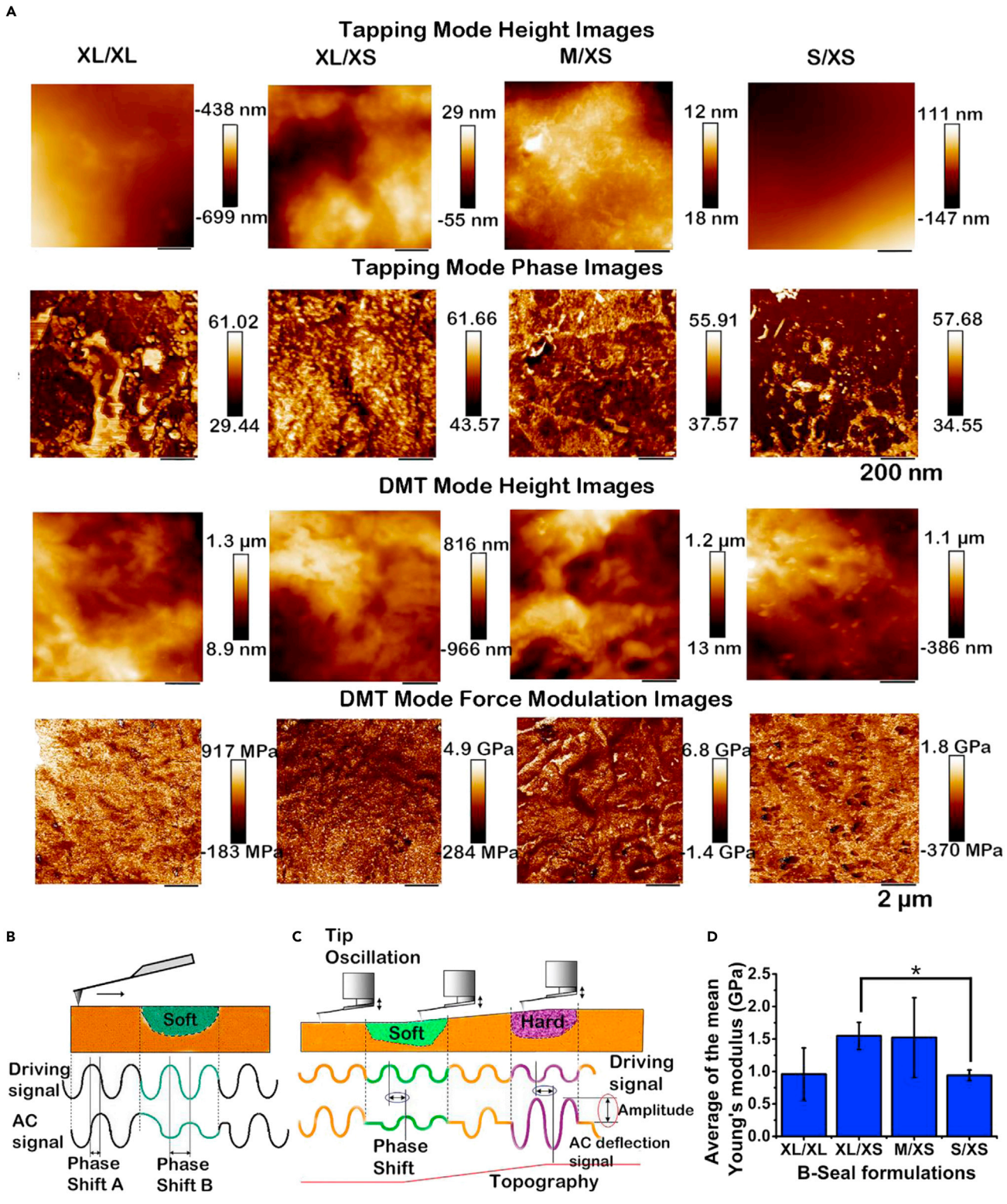

Figure 3. Mismatched particle sizes enhance the particles interfusion, penetration, and distribution

(A) AFM tapping mode for height (first row) and phase (second row) images of B-Seal film formed by the selected particle size pairs; scan size: 1 × 1 μm; cantilever: AC240TS standard Si cantilever (spring constant 2 N/m, resonance frequency 70 kHz); set point ratio 0.7; the z-scales for the phase and height images are 25° and 10 nm, respectively. AFM PeakForce quantitative nanomechanical mapping mode for height (third row) and phase (fourth row)

Figure 3. *Continued*
images of B-Seal film formed by the selected particle size pairs; scan size: 10 × 10 μm; cantilever: AC160TS standard Si cantilever (spring constant of 42 N/m, resonance frequency 300 kHz); set point ratio 0.7–0.8; the z-scales for the phase and height images are 25° and 10 nm, respectively.
(B and C) Schematic representation of the phase lag changes depending on the mechanical properties of the sample surface.
(D) The average of the mean Young's modulus of B-Seal films formed by the selected particle size pairs (n = 5, *p < 0.05).

Lap shear tests further supported the size effects, as shown in Figure 2F. XL/XS consistently showed the highest lap shear strengths. Following the increase of WPU (−) particle size and the decrease of WPU (+) particle size, the lap shear strength decreased accordingly, which is in agreement with the burst pressure results. XL/XS and M/XS were the strongest in lap shear strength compared with others. Further, the selected size pairs of XL/XS, M/XS, and S/XS were subjected to a T-pull test, as shown in Figure 2G. XL/XS, M/XS, and S/XS all showed similar T-pull strengths. B-Seal also showed minimal swelling behavior, with less than 10% after soaking in PBS at 37°C, as shown in Figure 2H. The minimal swelling and the sustained burst pressure in water for 5 days (Figure 1F) suggest that B-Seal may potentially maintain a long-lasting adhesion and seal in a wet condition. Meanwhile, the effect of volume ratio of A-B formulation was also investigated, as shown in Figure 2I. It appears that the 1:1 volume ratio of component A and component B has the best performance in burst pressure tests. Moreover, the influence of WPU (+) and WPU (−) concentrations on burst strength was investigated, as shown in Figures S4A and S4B. By reducing the concentrations of WPU (+) and WPU (−), burst pressures were decreased accordingly, which shows the importance of keeping both WPU (+) and WPU (−) at a relatively high concentration of 45% and 34%, respectively. The densities of B-Seal of all size pairs investigated are almost the same, suggesting the size variations do not alter the overall densities of the B-Seals (Figure S4C).

Atomic force microscopy characterization on adhesion mechanism

Atomic force microscopy (AFM) was utilized to explore the particle permeation, A-B phase interfusion, and mechanical properties of B-Seal at the nanoscale. In phase mode imaging, the phase shift of the cantilever oscillation was compared with the driving signal. Different samples exhibit various interactions with the AFM tip; hence, the corresponding phase shift is altered. The use of this mode is sometimes the only way to show differences between local regions on the sample. Figure 3A (first and second rows) shows the representative tapping mode AFM height and phase images of B-Seal with various particle size combinations. These phase images appear dramatically different among the group of B-Seals investigated. XL WPU (+) and M WPU(+) contain a large content of hard segments contributing to a large, discontinuous phase with bright color.

On the contrary, S WPU (+) and XS WPU (−) contain more soft segments, thus contributing to a continuous dark phase, which is evident for S/XS. The efficiency of A-B particles packing and interfusion during mixing can be characterized through the hard-soft segment distribution. Compared with XL/XL and S/XS, XL/XS and M/XS exhibit more evenly distributed phase images with scattered soft-hard segments. Obviously, the larger mismatched sizes of A-B particles result in better particle packing and interfusion. Therefore, particle packing and interfusion have significantly impacted the localized phase morphologies observed with AFM.

In force mode imaging (Derjaguin-Müller-Toporov model [DMT]), repulsive forces between the sample and the tip were used to investigate the B-Seal film properties. The tip was oscillated at a high frequency and moved to a distance at which the

repulsive forces acted. Sample elasticity can be calculated by using different theoretical models. The DMT generates a map of the sample's elastic properties from the changes in the amplitude of cantilever modulation. This mechanical mapping gives a very detailed insight into the nanoscopic morphology, revealing a broad distribution of surface moduli of the segmented polyurethanes, and a mean value can then be calculated from the distribution corresponding to an arithmetic average. Such measurements are especially interesting for A-B component film, because local variations can be calculated as well, which are illustrated in Figure 3B. The variation of the surface moduli over multiple scanned areas was determined and the DMT modulus values were described by modulus distribution functions.[31] The results are summarized in Figure 3D. Values determined as the average of the mean moduli were between 0.5 and 2.5 GPa. XL/XS and M/XS showed higher modulus at about 1.5 GPa whereas XL/XL and S/XS were lower at about 1 GPa. It should be noted that the values of AFM mechanical properties measured at the nanoscale should not necessarily coincide with the value of the same properties at the macroscale.[32] The stress applied on soft materials, such as polymers in AFM measurements, is between one and two orders of magnitude higher than the one applied on bulk measurements.[32] Our results are within the range of DMT modulus (1–2.2 GPa) of polyurethane measured by AFM in the previous studies.[31,33] The AFM studies further support that particle size mismatch in B-Seal contributes to the efficient particle packing and results in improved mechanical properties.

Microscopic observation of the porcine tissue interfaces bonded by B-Seal

To further explore the adhesion mechanism of B-Seal, the morphology of the interface of the B-Seal bonded porcine tissues was closely examined under the microscope (Figure S5). An apparent gap between XL/XL B-Seal and the surrounding tissue was observed due to the difficulty of large particles to penetrate/permeate on the tissue surfaces and the inefficient ionic cross-linking and particle packing/interfusion to interlock with the tissue surface. The rest of the size pairs in Figure S5 all showed promising tissue-glue bonding and interlocking with full integration of B-Seal with the surrounding tissues. However, the mass volume of the XS (+)/XS (−) group seemed less remained at the glue/tissue interfaces, which was ascribed to the possible partial infiltration of small particles into tissues before the glue sets, leading to less cured glues remained at the interfaces and relatively weaker mechanical properties compared with XL/XS and M/XS. Porcine tissues showed autofluorescence to distinguish from B-Seal under fluorescence microscopy with a 4′,6-diamidino-2-phenylindole (DAPI) filter. The morphology observation at the bonded tissue interfaces supported that the fast permeation and infiltration of nanoparticles enabled efficient glue-tissue interactions and facilitated the formation of mechanical interlocking via particle packing, interfusion, and ionic cross-linking.

In vitro cytotoxicity evaluation

In accordance with a minimal essential medium (MEM) elution assay (International Organization for Standardization [ISO] 10993-5), MEM elution from B-Seal at different gelling times (0 min, 2 min, and overnight with or without filtration using 0.2 μ m filters) were co-cultured with a mouse fibroblasts L929 cell line. All groups showed a viability greater than 80% of the control group (no elution supplemented), as shown in Figure S6A. Therefore, B-Seal is considered non-cytotoxic, according to ISO 10993-5, which defines that reduction of cell viability by more than 30% is considered a cytotoxic effect. At every elution, cytotoxicity tests for degradation products in Figure S6B showed no statistical difference in cell viability between B-Seal and a commonly used degradable polymer, polylactic acid (PLA). All groups showed above 80% viability.

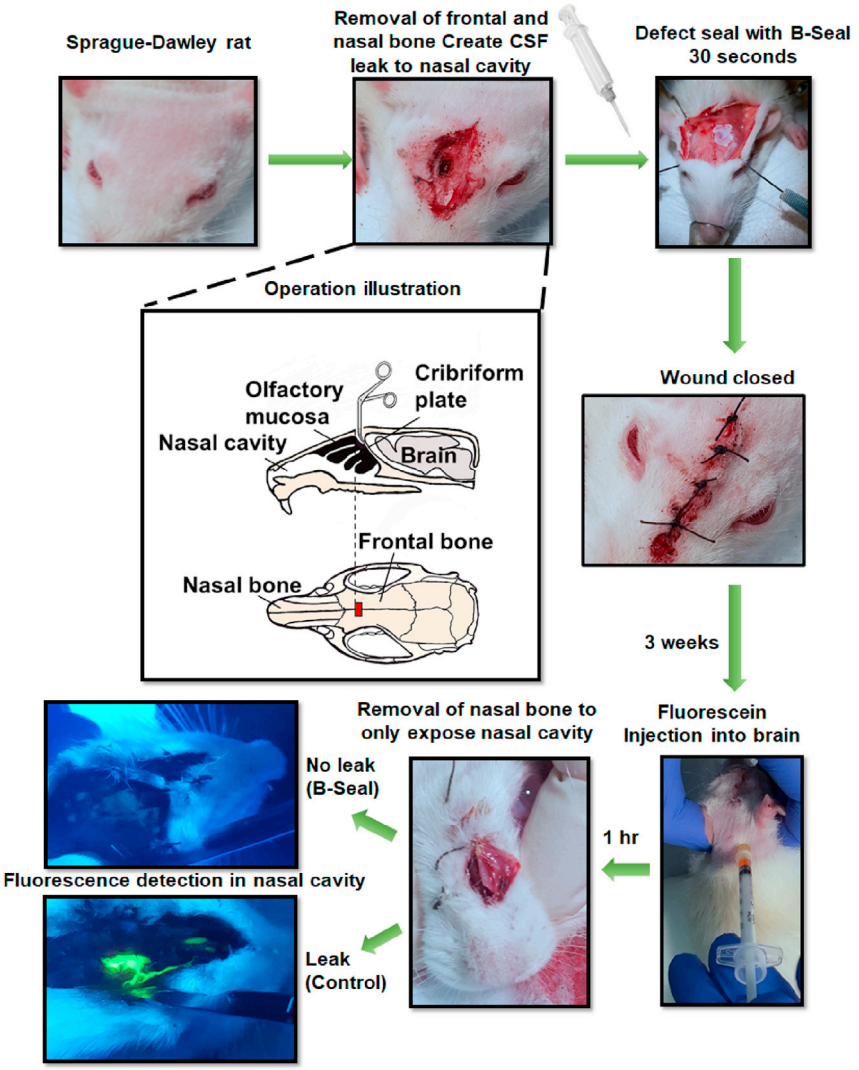

Figure 4. CSF leak prevention by B-Seal on a rat CSF rhinorrhea model

In vivo evaluation via a rat CSF rhinorrhea model

A Sprague-Dawley rat CSF rhinorrhea model was used to evaluate the feasibility of using B-Seal for CSF leak repair.[34] As shown in Figure 4, the cribriform plate that separates the olfactory bulb from the nasal mucosa anteriorly was penetrated with a metal-tip tool to open the space between the brain and the nasal cavity to create a significant CSF leak. B-Seal was applied to the defect using pipettes. An equal volume of A and B totaling 40 μL of solution was used to fill the cavity. Three weeks following implantation, 50 μL of fluorescein was injected into the cisterna magna to introduce fluorescence throughout the central nervous system (CNS). The rats were sacrificed and the spinal cord showed strong fluorescence under black light, demonstrating the successful fluorescein injection in the CNS. The nasal mucosa was subsequently dissected and also analyzed under black light for fluorescence. The nasal mucosa of the control rats in which the cribriform defect had not been repaired with B-Seal exhibited intense fluorescence in the mucosa. The mucosa of the rats that were treated with the B-Seal showed no fluorescence, demonstrating effective repair of the CSF leak. Noteworthy, the B-Seal was well integrated with the

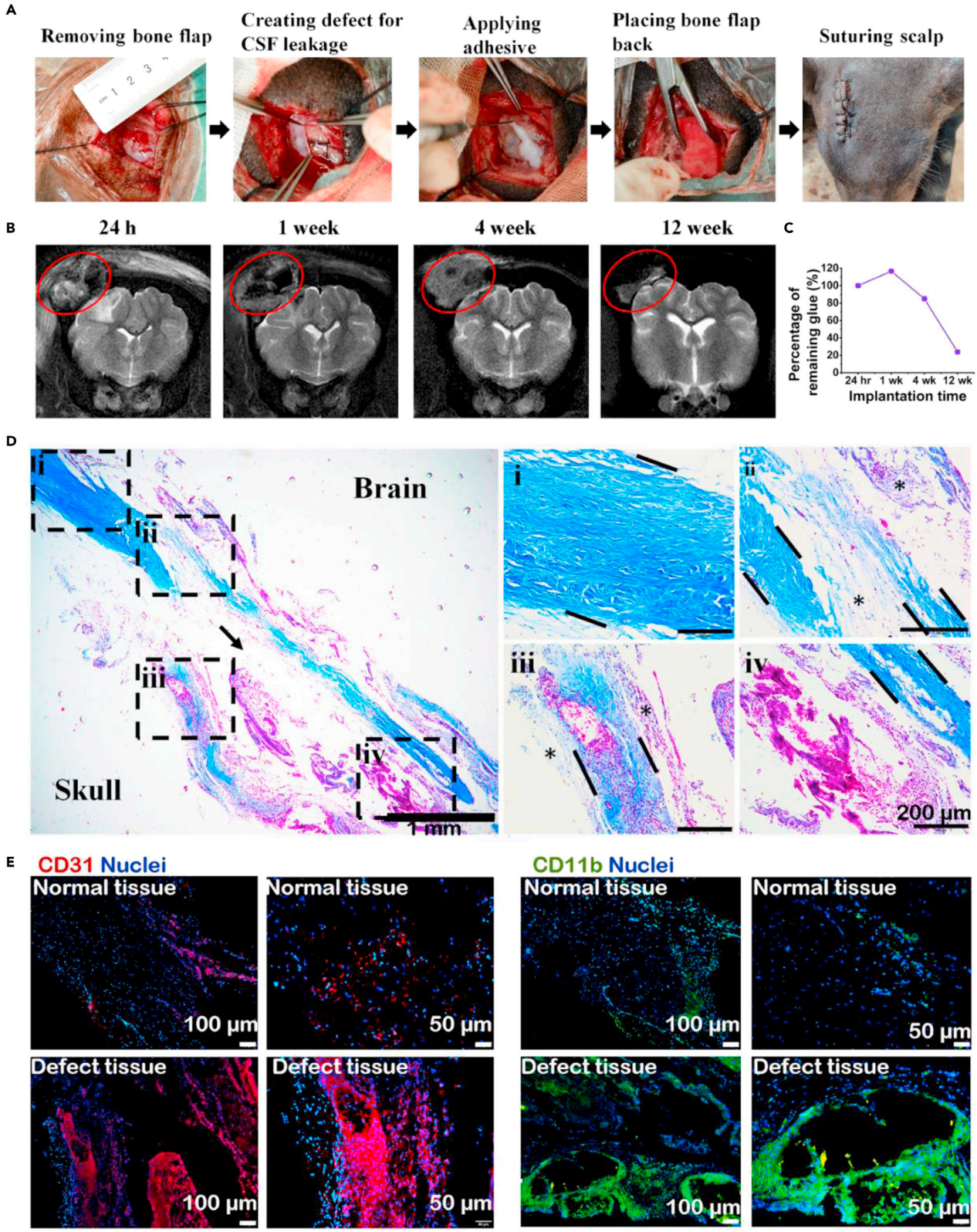
A
Removing bone flap
Creating defect for CSF leakage
Applying adhesive
Placing bone flap back
Suturing scalp
B
24 h
1 week
4 week
12 week
C
Percentage of remaining glue (%)
120
100
80
60
40
20
0
24 hr
1 wk
4 wk
12 wk
Implantation time
D
Brain
Skull
i
ii
iii
iv
1 mm
200 μm
E
CD31 Nuclei
CD11b Nuclei
Normal tissue
Defect tissue
100 μm
50 μm

Figure 5. Porcine craniotomy model for dura repair using B-Seal

(A) Surgical procedures of porcine craniotomy model.

(B) MRI T2-weighted images of pig brain at 24 h and 1, 4, and 12 weeks post-surgery. Red circle: B-Seal.

(C) Quantitative result of remaining B-Seal material volume changes over implantation time.

(D) Masson's trichrome staining of the harvested dura mater after 12 weeks of B-Seal implantation (magnifications: 40× and 100×; →: B-Seal created void; *: organized connective tissue).

(E) The tissues were stained for CD31 (red) and CD11b (green). Nuclei were stained with DAPI and are shown in blue.

surrounding tissues, and it was even hard to be pulled out using forceps. The tissues surrounding the implant appeared healthy. There were no redness, swelling, and tissue necrosis observed.

In vivo evaluation via a porcine craniotomy model for dural repair

A Chinese domestic miniature pig craniotomy model was used to evaluate the application of B-Seal for dural repair. Briefly, the animal had an approximately 3 × 2 cm bone flap removed from the left frontoparietal region of the skull. An approximately 2 cm incision was made through the dura and the arachnoid so that CSF was allowed to freely egress. Once leakage was verified, the dura was loosely approximated with a 6-0 suture, leaving an approximately 2 mm gap. B-Seal was applied to a depth of 1–2 mm to seal the leaking dura and the wound was then closed after the bone flap was placed back, as shown in Figure 5A. Magnetic resonance imaging (MRI) results (Figure 5B) showed that B-Seal was prominent in 24 h MRI image (red circle). There was some subdural fluid accumulation possibly caused by surgical procedure at 24 h. However, subdural fluid accumulation was not prominent at 1 week, suggesting the B-Seal implantation did not generate significant inflammation or any noticeable adverse effects.

Further water absorption by the B-Seal may also occur, evidenced by an MRI image of the B-Seal at week 4. The size and thickness of the materials did not change significantly 1 week post-implantation, suggesting the non-swelling properties of B-Seal, consistent with the *in vitro* swelling data (Figure 2H). Moreover, the volume of B-Seal was decreasing over time and there was about 22% of B-Seal remained at 12 weeks, suggesting that B-Seal was degrading but not fully absorbed yet (Figures 5B and 5C). There were no CSF leaks observed. After 12 weeks, the pig was sacrificed, and an independent veterinary pathologist examined the surgical site and found no visible fluid accumulation under the scalp and no noticeable CSF leak through the newly generated dura mater.

The harvested dura mater was stained with Masson's trichrome, as shown in Figure 5D. After 12 weeks of implantation, the healing of the damaged dura tissues seemed almost complete, with dense connective dura-like tissues (Figure 5D, dotted box areas) that stained positive for collagen type I (Figure S7), bridging the durotomy edges (from area ii to iv; area i is the normal dura tissue). By immunostaining of CD31, the formation of massive new blood vessels was evident in the newly regenerated dura-like tissue, and around the remaining B-Seal (arrow), but not within native dura tissue, indicating the degrading materials triggered an active healing process. Inflammation was noted in the newly regenerated dura-like tissue, revealed by immunostaining of the CD11b-positive macrophages. Moderate infiltration of the CD11b-positive macrophages was present, but mainly displaying a diffusing pattern around the newly generated blood vessels (Figure 5E), indicative of a normal immune response to degrading materials and wound healing. There was no evidence of excessive formation of fibrotic tissue and scar tissue, or tissue necrosis at the macrophage abundant sites. The macrophages presented around the remaining B-Seal should contribute to the clearance of the degrading materials.

Although the degradation of the above B-Seal was still not completed, these results confirmed the safety and efficacy of B-Seal for dura repair on a large animal model.

DISCUSSION

Each year, 1.7 million people in the US experience a traumatic brain injury, the primary cause of dural damage and subsequent CSF leaks. CSF leakage and its associated bacterial meningitis are the major causes of high morbidity and mortality in neurosurgery.[35] An intracranial pressure greater than 14.7 mm Hg (1.96 kPa) is able to cause CSF to leak through even small suture holes created during dural repair.[36] In order to prevent the leakage, a suitable dural glue needs to have sufficient adhesive and burst strength. Sealants are the most promising and convenient among CSF leak repair products, such as dura sutures, patches and grafts, and sealant and combinations thereof.[37] Current commercially available sealants include fibrin glues,[38] such as Tisseel and Evicel (used in ~52% of dura repairs), and synthetic polymer or protein-based products, such as DuraSeal and Adherus Autospray Dural Sealant.[39,40] Traditional sealants lack sufficient wet tissue adhesion strength and elasticity,[2] properties important in a dynamic, biological environment. In addition, the ability to accommodate such variables as intracranial pressure fluctuations, gradual material degradation, and progressive tissue regeneration is required to achieve healthy tissue integration and a reliable seal.[8,41]

Fibrin glue exhibits weak wet tissue adhesion strength, a risk for viral transmission and allergic reactions, and expensive and troublesome production and preparation processes. The adhesion strength of fibrin glue is only approximately 20 kPa and its quick degradation onset rapidly decreases the adhesion strength over a short period of time when used alone, posing a high risk for CSF leak.[42,43] Therefore, fibrin glue is often used as an adjuvant dural sealant to reduce the leakage in combination with other materials/devices, such as vascularized nasal tissue flaps or collagen-based patches in duraplasty. Synthetic polymers like the PEG-based DuraSeal have high swelling ratios (~400%), which pose a serious risk to CSF leak and the maintenance of intracranial pressure.[16,44] Due to the limited adhesive strengths and elasticity, the current products cannot provide a long-lasting dural seal capable of withstanding intracranial pressure. The inert PEG-based materials are also not conducive to tissue repair. The newly developed Adherus Autospray Dural Sealant has a more favorable swelling ratio (~46%) than DuraSeal. Still, it uses a relatively toxic secondary component, polyethyleneimine (PEI), which disrupts the cell and mitochondrial membranes, leading to necrotic and apoptotic death.[40] The post-operative CSF leaks increase the risk of intracranial infection, leading to meningitis, an often fatal condition.[45] CSF leak may occur way before the adhesives or sealants completely degrade. Swelling and partial degradation of the applied sealants may contribute to the adhesion failure and CSF leak. Other than strong wet adhesion, the ideal dura sealant should also be safe and biodegradable. Although there is no consensus on exactly how long a bioadhesive should degrade for dura repair, the ideal adhesive should maintain mechanical integrity long enough to allow the dural tissues to heal without posing a risk of premature implant failure and post-surgical leak. Therefore, there is an urgent need to develop a more reliable dura repair adhesive sealant capable of maintaining a strong and watertight seal to address both the high leak incidence rate and the tissue repair challenges associated with CSF leak management.

Because the primary purpose of B-Seal sealant is to provide a watertight seal, it is important to confirm if B-Seal can seal wet tissues throughout the healing process

while withstanding physiological pressures. In general, cranial CSF pressures average approximately 15 mm Hg and spinal CSF pressures average approximately 30 mm Hg, with pressure spikes that may reach at least 45 mm Hg. An approximately 1-mm-thick layer of B-Seal sealant was able to withstand an average burst pressure well over three times the hyper-physiological levels that may be generated in the spine, with an average burst pressure of 198.33 mm Hg (26.44 kPa, Figure 1C). Furthermore, B-Seal maintained significant burst strengths (>45 mm Hg/6 kPa) even after 4 weeks of incubation in PBS (Figure 1F). This is an important feature of B-Seal that is critical for preventing the premature failure of the adhesive sealants on wet tissues. B-Seal also showed minimal swelling behavior, with less than 10% swelling versus around 400% of swelling of PEG-based DuraSeal sealant,[16,44] after soaking in PBS at 37°C, as shown in Figure 2H, supporting the hydrophobic nature of polyurethane-based B-Seal. The minimal swelling and the sustained burst pressure in water over time (Figure 1F) explain its long-lasting adhesive and sealing capability in wet conditions and make B-Seal ideal for many surgical applications.

Surgical adhesives are often used in surgical situations where the damaged tissues are under constant movements or deformation or tissue friction. Constant tissue movements very likely contribute to the failure of tissue bonding due to the weak cohesive and adhesive strength of the tissue adhesives used. Unfortunately, most tissue adhesives, such as Dermabond, DuraSeal, and Tisseel, are incapable of balancing a strong adhesion strength, a strong cohesive strength and a considerable elasticity. Thus, they are not suited in applications where constant tissue movements occur. For all the mechanical tests in Figure 1, the ultimate failures of B-Seal were due to the separation of B-Seal from tissues, unlike the DuraSeal, and Tisseel that were failed due to the failure of materials themselves, suggesting B-Seal is strong in both adhesion and cohesion. The strong but elastic nature (Figure 1H) of B-Seal enables the glue to maintain an excellent adhesion in a dynamic tissue movement situation thus is considered as a favorable feature for tissue closure. It should be noted that the lap shear strength of the strongest commercial tissue adhesive, Dermabond (CA) is around 80 kPa,[14] and it is cross-linked by toxic chemical bonding. Our exciting results showed that B-Seal is the first aqueous, super-strong, and elastic tissue adhesive demonstrating equivalent lap shear strengths (83.67 $\pm$ 12.92 kPa, Figure 1E) to Dermabond (CA) without using any toxic chemical cross-linking.

Previous studies have shown that only 6% of conventional sutured closures in cranial and spinal procedures were watertight.[46] To address this problem, non-toxic and biocompatible hydrogel sealants were applied along with sutures in order to provide watertight closure. Indeed, a hydrogel itself has remarkable cohesion, while its adhesion to another material is weak, especially under wet conditions.[47,48] A hydrogel in nature is an aggregate of water and polymers, with the water the major component and polymer the minority. The abundance of water molecules in hydrogel weakens the adhesion to other materials. In order to improve the adhesion of polymeric sealants, rather than the inclusion of functional groups for covalent bonding, the synergy of topology and mechanics in non-covalent adhesion becomes critical.[49–52]

It was reported that the high surface adhesion energy might be achieved by energy dissipation through materials inside either the adhesive or the substrate,[2] which was inspired by slug adhesion where strong adhesion arises from two interpenetrating network of polymers.[53,54] Because the surfaces of tissues or cells are negatively charged, the energy can be effectively dissipated when the interface between adhesive and tissue is closely engaged via electrostatic attraction via a positively charged

amine-containing bridging polymer. The bridging polymer can further penetrate the target tissues, forming physical entanglement and a chemical anchor for covalent bonding. However, the concern is the covalent bonding involving carbodiimide coupling, which poses toxicity concerns on vital organs, such as the brain. Another idea is introducing photoactive groups such as azide,[55,56] diazirine,[57] and metal-ion complexes[58] in the compounds to form covalent bonds with tissue under UV. Although with fast curing and strong bonding, UV irradiation may also cause tissue damages.[59]

Mechanical interlock is a well-known mechanism of adhesion. For surfaces with rough topology, a liquid adhesive fills the asperities and then solidifies to a rigid adhesive layer that is interlocked and retained by the surface.[17] Mechanical interlock is normally weak due to the soft nature of material itself and can be damaged by deformation. However, if the material can permeate through the interconnected pores or fill in the asperities on the surface and harden quickly, the interlock can only be broken by rupture, which requires much more energy. Moreover, multi-species of polymer chains diffuse together, and the topological entanglement with the preexisting elastomer networks contribute to the topological adhesion. The feat of English ivy clinging on a wall or tree is very similar to mechanical interlock and topological adhesion. The plant secretes negatively charged nanospherical glycoprotein particles that intercalate and aggregate on a target surface. These nanoparticles form a penetrating film that is further strengthened via cross-linking by ion interaction with calcium ions, thus enabling mechanical interlocking between the roots of English ivy and the surface to which it clings.[60]

In another aspect, particle packing theory has been well applied to enhance the mechanical performance in the concrete industry. A concrete mix contains aggregate particles of various sizes. Maximizing the packing density is an efficient strategy not merely for the performance amelioration but also to influence the workability and flowability. As a binary mix of particles, shown in Figure 1B, if the sizes between coarse and fine particles were too close, the filling/packing effect would be hindered due to that the fine particles are not small enough to fit in the voids between coarse particles.[26] Ideally, the size difference between the coarse particles and the fine particles should reach a certain range where the so-called wedging effect occurs, from which filling particles are wedging to the voids to provide ultimate packing density. The wedging effect can be demonstrated in our formulation optimization tests, shown in Figure 2, where the optimal combinations may be chosen from WPU (+) groups with sizes larger than MS, preferably XL or L, and from WPU (−) groups with sizes smaller than MS, preferably S or XS, to achieve high burst pressure, if an ideal burst pressure value for a dural sealant is set to be above 80 mm Hg (10.67 kPa). By adopting this particle packing theory, the size difference between mismatched A-B particles induced the improvements of both mechanical strengths and particle interfusion of B-Seal, which can be confirmed by the mechanical tests and AFM nanoscopic observation in Figures 2 and 3.

Therefore, inspired by English ivy adhesion and particle packing theory, we rationally designed B-Seal as WPU nanoparticle dispersions with counterions in its A-B (WPU [+]/WPU [−]) formulation. Particle size and charge of nanoparticles are known to play an important role in the nanoparticle dispersion stability, the setting time, and adhesion strengths.[47,61] The WPU nanoparticle sizes can be tuned by varying the choices of monomers (hydrophilic or hydrophobic diols/diamines or combinations thereof) and processing conditions, such as reaction time, reaction temperature, shearing speed, and so on. Polyurethane is known for its robust and tunable

mechanical properties and has been widely used in many medical devices, such as medical tubing, pacemaker, and industrial coatings. When the counterions of the hydrophobic WPU dispersions were applied to the tissue surfaces, the efficient particle penetration into the rough tissues, such as compromised or damaged tissues, irreversible WPU nanoparticle interfusion, and the rapid ionic interactions of counterions accelerates the exclusion of water molecules from the interface of the B-Seal and the tissues to form a strong mechanical interlocking. Furthermore, the mismatched particle sizes of WPU (+) and WPU (−) further facilitated the packing and hardening process to achieve a strong adhesion. It should also be noted that the strong adhesion of B-Seal does not necessarily require nanoparticle penetration into the tissues. Micrometer-sized asperities on rough surfaces, such as uncompromised human skin (around 3 μm of roughness),[62] should accommodate the localization of B-Seal nanoparticle to form mechanical interlocking. The B-Seal nanoparticles do not necessarily have to penetrate through the surfaces. This notion is also supported by the strong lap shear adhesion tested on porcine split skins that contain the dense and compact epidermis layer (Figure 1D).

In vitro cytotoxicity and *in vivo* evaluation on a rat CSF rhinorrhea model and a porcine craniotomy model supported B-Seal's excellent safety and efficacy for CSF leak prevention and dura repair. The results clearly showed that B-Seal effectively sealed the leakage in rats and facilitated dura regeneration in pigs. MRI results (Figure 5B) showed no brain herniation at all time points, and dura tissues were healing without triggered significant inflammatory responses (Figure 5D). CD11b-positive macrophages, CD31-positive endothelia cells, and new collagen production were evident in the regenerated tissue, indicating an active healing process (Figures 5E and S7). Meanwhile, no apparent adhesions between the implant and the cortex were observed. Although the B-Seal was not fully degraded as observed by MRI and in histology at week 12 (Figures 5B–5E), aqueous B-Seal must be stable or have very slow hydrolysis for extended shelf life (>1year) but relatively fast degradation *in vivo* (2–4 months) for dural repair. The *in vitro* degradation for B-Seal in PBS for 15 weeks is almost negligible (0.14%) (Figure S3F), suggesting that B-Seal is very stable and should have more than 2 years of shelf-life. *In vitro* oxidative and enzymatic conditions accelerated the B-Seal degradation (Figure S3F). However, *in vitro* degradation conditions do not fully replicate the *in vivo* environment. It is also known that degradable polyurethanes degrade much faster *in vivo* than *in vitro* because polyurethanes are susceptible to enzymatic and oxidative degradation *in vivo* as cells, such as macrophages, secrete various enzymes and/or oxidative species. Quantitative MRI measurements and histological analyses (Figures 5B–5E) suggested that B-Seal only had about 20% remained after 12 weeks post-surgery. The results supported the notion that the adhesive should degrade at a reasonable rate that would allow a health dura repair but avoid premature dura healing or CSF leakage before its complete degradation. The B-Seal would continue resolving as evidenced by the moderate infiltration of vascular cells and macrophages over the healed dura tissues. It should be noted that the conventional bioglues, such as DuraSeal and Tisseel, are usually used as adjuvants to other tissue grafts or duraplasty devices. In the present study, B-Seal served well not only as an adhesive sealant to prevent CSF leak but also as a scaffold or a synthetic graft to aid in dura repair without using additional tissue grafts or duraplasty devices.

In summary, we have rationally developed a unique polyurethane nanodispersion-based B-Seal tissue adhesive. B-Seal is the first fully synthetic biodegradable aqueous wet tissue adhesive without using any toxic chemical cross-linking. B-Seal offers advantages over the existing tissue adhesives and sealants, including its fast

tissue adhesion, super-strong wet tissue adhesion strengths, tenacity and flexibility, long shelf-life, and excellent *in vivo* safety and efficacy for CSF leak prevention and dura repair. The design strategy that uniquely combines English ivy adhesion mechanism and particle packing theory to achieve unparalleled wet tissue adhesive strengths represents a new direction in designing the next generation of tissue adhesives and sealants to address the challenging problems related to leak prevention and tissue regeneration in various surgeries.

EXPERIMENTAL PROCEDURES

Resource availability

Lead contact

Further information and requests for resources and reagents should be directed to and will be fulfilled by the lead contact, Chao Liu (ch.liu@aleobme.com).

Materials availability

This study did not generate new unique reagents.

Data and code availability

The data generated during the study are available from the corresponding authors on reasonable request.

Materials

Polycaprolactone diol (PLACCEL210; molecular weight, 1000) and acetone (99.7%) were purchased from Daicel Corporation (Tokyo, Japan) and Fisher Scientific (Pittsburgh, PA), respectively. IPDI (98%), MDEA (99%), and EDA (99.5%) were all purchased from Acros Organics (Fair Lawn, New Jersey). Tin(II) 2-ethylhexanoate, Sn(Oct)2 (95.2%), and BDO (99%) were purchased from Sigma-Aldrich (St. Louis, Missouri), while DMPA (98%) and 2-dimethylaminoethanol (DMAE; 99%) were purchased from Alfa Aesar (Ward Hill, Massachusetts). All the chemicals are used as received unless otherwise stated.

WPU syntheses

B-Seal is designed as an A-B formulation with WPU (+) nanodispersion as component A and WPU (−) nanodispersion as component B. Biodegradable WPUs were synthesized using PCL-diol and aliphatic diisocyanate IPDI as the main reactants, BDO and EDA as the NCE, and DMPA (for WPU [−]) or MDEA (for WPU [+]) as the ICEs. $Sn(Oct)_2$ was used as a catalyst. To synthesize WPU (+), PCL, MDEA, and $Sn(Oct)_2$ were melted and dried under vacuum (40 mm Hg) at 90°C for 2 h, with a continuous stirring in a 100 mL two-neck round-bottom flask. After reducing the temperature to 60°C, IPDI in 15 mL dried acetone was added and the reaction was continued at 60°C for a predetermined time (NCO/diol/ICE reaction time). After the reaction, the polymer solution was transferred to a 250 mL beaker, and EDA in 10 mL dried acetone was added as a chain extender to react with the unreacted isocyanate (−NCO) terminal groups; 5 mL 1 M HCl was added in the beaker under stirring to convert MDEA into quaternary ammonium salt. Next, 15 mL deionized (DI) water was slowly dropped in the beaker under a stirring speed of 1000 rpm for 30 min, followed by acetone removal using a rotary evaporator to obtain the final WPU (+) nanodispersion. To synthesize WPU (−), PCL and $Sn(Oct)_2$ were melted and dried under vacuum (40 mm Hg) at 90°C for 2 h, with a continuous stirring in a 100 mL two-neck round-bottom flask. After reducing the temperature to 60°C, IPDI was added to the flask to continue the reaction at 60°C for 1 h. DMPA and BDO in 5 mL dried acetone was then added to continue the reaction for a predetermined time. Next, the polymer solution was transferred to a 250 mL beaker, EDA and DMAE were then added

under stirring, and then 35 mL DI water was slowly dropped in under a continuous stirring at 1000 rpm for 30 min, followed by acetone removal to obtain WPU (−) dispersions.

Particle size and zeta potential

The particle size and zeta potential of both WPU (+) and WPU (−) nanodispersions were determined using a Zetasizer Nano ZS (Malvern Instruments, Malvern, UK). The measurements were conducted according to the standard operation procedure (SOP) and a quick start guide provided by the manufacturer. For both WPU (+) and WPU (−) nanodispersions with a solid content in the range of 30–50 wt %, 1000× dilution of samples was measured at 25°C.

Burst pressure test

Burst strength test was conducted according to ASTM F2392-04. The collagen casing roll (Nippi Casing [#320], Burnaby, British Columbia, Canada) was cut into a 38 × 38 mm piece, washed in deionized water to remove glycerin, and then soaked in fresh deionized water for 5 min. At the center of the rectangular collagen casing substrate, a 3.0 mm diameter hole was created using a hole puncher. The B-Seal, containing 200 μL A (WPU [+]) and 200 μL B (WPU [−]), respectively, was applied and mixed instantly to seal the hole on the substrate. The adhesive sealant was allowed to gel for 10 to 15 min before the substrate was placed in PBS and incubated in an environmental chamber at 37°C for 3 h followed by conditioning at ambient temperature for 15 min. Then, the substrate with the gelled B-Seal was placed onto the fixture base of a burst pressure test device, with the B-Seal facing up. The O-ring (internal diameter = 22 mm) was then placed on top of the tissue to secure the fixture top in place. The peak pressure was recorded as the maximum burst pressure. Commercial adhesives, DuraSeal (Integra LifeSciences, Plainsboro, New Jersey) and Tisseel (fibrin glue) (Baxter Healthcare, Westlake Village, California) were used as controls ($n \geq 5$).

Lap shear test

The lap shear test was conducted according to ASTM F2255-05. Frozen split porcine skin that has been aseptically prepared was used in the test. The tissue was bonded to the specimen holder with a superglue (Henkel, Bridgewater, New Jersey). The substrate was cut into a size of 1 × 2.5 cm^2 using a template and a fresh scalpel blade. The B-Seal, containing 200 μL A (WPU [+]) and 200 μL B (WPU [−]), was applied to the substrate surface and mixed homogeneously to form a uniform coating between the substrate surfaces. B-Seal, consisting of 200 μL A (WPU [+]) and 200 μL B (WPU [−]), formed an adhesive layer with a thickness of around 200 μm. A force of approximately 1 to 2 Newton (N) was applied to the bond area until the adhesive gelled. After conditioning in an environmental chamber at 37°C for 1 h 15 min and covered with wet towel paper, all specimens were further conditioned at the test temperature for 15 min before testing. The test specimens were placed in the grips of the testing machine (Instron model 5966, equipped with a 10 N loading cell) so that the applied load coincides with the long axes of the specimens. Force was applied to the specimen until failure at a constant cross-head speed of 5 mm/min. The load at failure (maximum load sustained) was recorded ($n \geq 5$).

T-pull test

The T-pull test was conducted according to ASTM F2258-05. Similar to the lap shear test, the tissue was bonded to the specimen holder with a superglue. The substrate was cut into a size of 2.5 × 2.5 cm^2. The B-Seal containing 200 μL A (WPU [+]) and B (WPU [−]) was applied to the substrate surface and mixed homogeneously to form a

uniform coating between both substrate surfaces. A T shaped specimen holder was clamped to ensure the bonded area with adhesive was entirely gelled. After conditioning in an environmental chamber at 37°C for 1 h 15 min, all specimens covered with wet towels were stabilized at the test temperature for 15 min before testing. The test specimens were then placed in the grips of the Instron testing machine (model 5966) so that the applied load coincides with the long axis of the specimen. Force was applied to the specimen until failure at a constant cross-head speed of 2 mm/min. The load at failure was lastly recorded ($n \geq 5$).

Ex vivo tissue bonding examination

Porcine meat purchased from a local butcher store was utilized to study the interface bonding between B-Seal and tissue. Briefly, the porcine meat specimen (dimensions: 40 × 40 × 40 mm) was cut in the middle to create a deep defect. B-Seal (200 μL A (WPU [+]) and 200 μL B (WPU [−])) was injected into the defect to seal the defect. After curing B-Seal for 1 h, the specimen with B-Seal was trimmed, embedded in Cryomatrix (Thermo Scientific, Waltham, Massachusetts), and cryosectioned into 5 μm sections with an ultramicrotome (PowerTome PC, Boeckeler Instruments, Tucson, Arizona). The interface between B-Seal and tissue was observed under an optical/fluorescence microscopy (Eclipse Ti-U, Nikon, Tokyo, Japan).

AFM

To study the particle permeation at the nanoscale, B-Seal film specimens were embedded in Cryomatrix (Thermo Scientific, Waltham, Massachusetts) and cryosectioned to obtain a smooth cross-section of the films for AFM observation. For all AFM specimens, the root-mean-square roughness of the surface was less than 3.5 nm. Tapping mode AFM imaging of all specimens was performed on a Bruker Dimension Icon AFM system (Bruker Optics, Billerica, Massachusetts) at ambient conditions. Images were captured at a set point ratio of 0.7–0.8. AC160TS standard Si cantilever (spring constant of 42 N/m, resonance frequency 300 kHz) was used for PeakForce quantitative nanomechanical mapping of specimens. AC240TS standard Si cantilever (Asylum Research, Santa Barbara, California) (spring constant of 2 N/m, resonance frequency 70 kHz) was chosen for tapping mode with phase imaging of specimens. The average of the mean Young's modulus of specimens ($n = 6$) using the NanoScope Analysis 2.0 software were analyzed.

ATR-FTIR and ^{1}H-NMR

FTIR spectra were acquired with a Nexus Thermo Nicolet spectrometer (Thermo Scientific, Waltham, Massachusetts) equipped with ATR device in the range of 450 to 4000 cm^{-1} with a resolution of 4 cm^{-1}. Films of component A, component B, and B-Seal were all characterized. The ^{1}H-nuclear magnetic resonance (^{1}H-NMR; 300 MHz) spectra were obtained using a Bruker DRX 400 spectrometer (Bruker Optics, Billerica, Massachusetts). The test samples were cast on a polytetrafluoroethylene (PTFE) dish, air-dried for 24 h, and then dried under vacuum for another 24 h to form a film. For NMR, 10 mg of the dried polymer film was dissolved in 0.6 mL deuterated DMSO-*d6*, and sonicated for 5 min to ensure that the film was completely dissolved.

Swelling test

To measure water uptake, sample plugs were created by pipetting B-Seal (A-B solutions) into a Teflon mold (length × width × height = 9.5 × 7.8 × 2.5 mm), pressed into film after mixing, followed by drying under ambient and vacuum conditions. The B-Seal plugs ($n \geq 5$) were weighed immediately after creation. The samples were weighted after soaking in PBS (pH 7.4) at 37°C for 1, 5, and 12 days and then weekly

thereafter. As described elsewhere,[63] the following formula was used to calculate the percent swelling:

$$\%S = \frac{(m_1 - m_0)}{m_1} \times 100\%$$

where %S = the percent swelling; m_1 = the mass at a given soaking time; and m_0 = the mass before soaking.

Density measurement

The density of B-Seal films was measured via a Mettler Toledo balance density measurement kit (Mettler Toledo, Columbus, Ohio). The B-Seal films were weighed in air (A) and then again in the auxiliary liquid with a known density (B). The density of the solid ρ can be calculated as follows:

$$\rho = \frac{A}{A - B}(\rho_0 - \rho_L) + \rho_L$$

where ρ = density of the sample; A = weight of the sample in air; B = weight of the sample in the auxiliary liquid; ρ_0 = density of the auxiliary liquid; and ρ_L = density of air.

Hydrolytic, enzymatic, and oxidative degradation

For hydrolytic degradation, B-Seal samples were first dried under vacuum and then 50 mg dried samples (n = 6) were incubated in 1 mL PBS at 37°C. At each time point, samples were removed from PBS, rinsed with deionized water, dried under vacuum for 48 h, and then weighed for up to 16 weeks. For enzymatic degradation,[64] 50 mg dried samples (n = 6) were incubated in 1 mL PBS containing 1 U/mL of CE at 37°C. The enzymatic degradation medium was replaced every 3 or 4 days to maintain enzyme activity and the mass loss was measured at predetermined times for 16 weeks. For oxidative degradation, 50 mg dried samples (n = 6) were incubated in an oxidative degradation medium comprising 20 wt % H_2O_2 and 0.1 M $CoCl_2$. The cobalt ion and H_2O_2 react to form hydroxyl radicals, simulating the oxidative radicals present at the material-macrophage interface.

In vitro cytotoxicity study

To assess the cytotoxicity of B-Seal, an MEM elution test was performed using L929 mouse fibroblast cells per ISO 10993-5:2009. L929 cells were cultured in Eagle's MEM with 10% fetal bovine serum (FBS) in a humidified atmosphere with 5% CO_2 at 37°C. To prepare the medium extract, 200 uL of the sterilized component A solution was mixed with 200 uL of the sterilized component B solution in 35 × 10 mm culture dishes. After 0 min, 2 min, and overnight, respectively, a complete culture medium was added to the culture dishes to incubate with the B-Seal for 24 h at 37°C with agitation. Next, the MEM extracts were collected and incubated with the L929 cells in 96 well plates for 24 h. MEM alone served as the negative control. Lastly, the cell viability was tested using Cell counting kit-8 (CCK-8; Dojindo, Rockville, MD), according to the manufacturer's instructions.

The cytotoxicity of the degradation product of B-Seal was also tested using L929 cells. To prepare the degradation product solution, 0.5 g B-Seal sample was first fully degraded in 9 mL 0.2 M NaOH, followed by pH adjustment to neutral using 1 M HCl. After centrifuged, the degradation product solution was sterilized by filtration. Degradation product solution of PLA was also prepared as the material control. Dilutions of the degradation product solution (2×, 5×, 10×, and 50×) with cell culture medium were prepared and added to incubate with L929 cells in 96 well plates.

Culture medium alone served as the negative control. The cell viability was tested using the Cell Counting Kit-8 (CCK-8; Dojindo, Rockville, MD), according to the manufacturer's instructions.

Rat CSF rhinorrhea model

A rat CSF rhinorrhea model was used to study the efficacy of B-Seal for CSF leakage prevention. The rat experiments were performed in compliance with a protocol approved by the Institutional Animal Care and Use Committee (IACUC) of Hershey Medical Center at the Pennsylvania State University. The 7-week-old Sprague-Dawley rats (both female and male) were anesthetized 30 min before the operation by a mixture of ketamine (20 mg/kg) and xylazine (2.0 mg/kg) at a 10:1 ratio through intramuscular injection. Once the animals were anesthetized, the top of the head was shaved, artificial tears were placed on both eyes, and betadine solution was spread over the skull's skin. A 2 cm sagittal incision was made to expose the skull, including the anterior cranial fossa. The area directly anterior to the naso-cranial suture on the right side was drilled through to the dura with a 1 cm drill bit. Once the dura and olfactory bulb were exposed, the olfactory bulb was aspirated for a distance of 2 mm. The cribriform plate that separates the olfactory bulb from the nasal mucosa anteriorly was subsequently damaged with a metal-tip tool to allow the accessible communication of the CSF between the brain and nasal cavity. Both male and female rats were randomly grouped for evaluating: (1) control with no glue and (2) B-Seal. B-Seal (A and B) was injected and mixed into the newly formed defect in the cribriform plate using syringes. At 3 weeks, the rats were injected with 50 μL of 0.0001% fluorescein into the cisterna magna to introduce fluorescence to the CNS. The fluorescein was allowed to circulate within the CSF for 1 h, and the rats were then sacrificed. The spinal cord was then analyzed under black light to determine for positivity of fluorescein in the CSF, demonstrating positive fluorescein injection in the CNS. The nasal mucosa and the surfaces where B-Seal was applied were analyzed under black light for fluorescence. The nasal mucosa of the rats that is not repaired with B-Seal should have intense fluorescence in the nasal cavity. The rat has no fluorescence in the nasal cavity demonstrates effective CSF leak prevention.

Porcine craniotomy model

An adult Chinese domestic pig craniotomy model was used to evaluate the safety and efficacy of CSF leak prevention and dura repair. The pig studies were performed in compliance with a protocol approved by the IACUC Committee of Kunming Medical University. The pig (~22 kg) was mounted on an operating table, anesthetized with sodium pentobarbital, at a dose of 40 mg/kg body weight via ear vein. Then, a linear skin incision was made in the right frontoparietal region. The muscle was dissected, and an approximately 3 × 2 cm bone flap was removed with a highspeed drill. Next, an approximately 2 cm incision was carefully made through the dura and the arachnoid so that CSF was allowed to freely egress. Once the leakage was verified, the dura was loosely sutured with 6-0 absorbable silk, leaving an approximately 2 mm gap. B-Seal itself is an aqueous solution. A small amount of fluid should not interfere the gelling and curing of the B-Seal. However, if the amount of physiological fluid is large enough to flush away or dilute the applied B-Seal solutions, it may affect the performance of B-Seal. Therefore, the surgical area was then gently tapped by a surgical gauze to partially remove the fluid before applying B-Seal. For B-Seal application, 2.7 mL of WPU (−) was applied to the dural surface, followed by adding 2.7 mL WPU (+) and mixed carefully for a few seconds. The bone flap was then placed back over the sealant and closed using 2-0 Vicryl sutures. The animals were anesthetized at 24 h and 1, 4, and 12-weeks post-implantation, and MRI scans were acquired using a 3T MRI scanner (Philips Achieva, the Netherlands). To quantify the volume changes of B-Seal over time, the Digital Imaging and Communications in

Medicine (DICOM) data were first exported to Mimics 21.0 (Materialise, Belgium) and then the axial position of the T2-weighted images was chosen to draw an outline of the B-Seal using multiple slice edit with proper threshold on Mimics 21.0. Finally, the 3D images of B-Seal were reconstructed, and the volumes of the B-Seal were measured.

At 12 weeks post-implantation, the pig was sacrificed and the dural skull bone was collected and fixed with 4% paraformaldehyde for 4 weeks. The skull bone was decalcified at room temperature for 3 months with 10% ethylenediaminetetraacetic acid (EDTA) solution under continuous and gentle shaking. The decalcifying solutions were changed once a week. Subsequently, the bone was washed 2 h using running tap water, followed by routine dehydration and paraffin embedding. Next, 5 μm sections were cut using a Leica microtome (Leica, Buffalo Grove, Illinois) and placed on glass slides. Finally, the sections were deparaffinized, rehydrated, and stained with Masson's staining (Masson's Trichrome Stain Kit, Solarbio, China).

To evaluate the CD31, CD11b, and collagen expression, the sections were deparaffinized and rehydrated, and the endogenous peroxidase activity was blocked with 3% H_2O_2 solution in methanol. Then, the sections were treated with 0.01 M sodium citrate buffer to retrieve the antigen, blocked with 5% normal goat serum for 1 h at 37°C, and subsequently incubated with the primary antibody for CD31, CD11b (Proteintech, China), and COL1 (Abcom, UK), respectively (1:200 diluted in 5% BSA solution) at 4°C overnight. For immunofluorescent staining, secondary antibodies CoraLite488-conjugated Goat Anti-Mouse IgG(H + L) and CoraLite594-conjugated Goat Anti-Rabbit IgG(H + L) (1:200 diluted) were incubated with sections for 2 h at room temperature, followed by nuclear staining and observed on a fluorescence microscope (BX53, Olympus, Japan). For immunohistochemical staining, sections were incubated with a reaction enhancer and secondary HRP-Goat anti-Rabbit IgG (ZSGB-BIO, China) for 30 min at 37°C. Positive staining was subsequently developed in DAB solution (diaminobenzidine tetrahydrochloride staining, Boster Biological Technology, China) and the sections were finally counterstained by hematoxylin.

Data processing and analysis

Outcome variables generated from these tests were summarized and expressed as mean ± SD. Normality and equality of variance were tested before a statistical test. The unpaired Student's t test was used for data analysis between two groups. One-way ANOVA followed by Tukey's *post hoc* test was used for multiple comparisons; $p < 0.05$ was considered statistically significant.

SUPPLEMENTAL INFORMATION

Supplemental information can be found online at https://doi.org/10.1016/j.matt.2021.12.018.

ACKNOWLEDGMENTS

The authors would like to acknowledge the partial support of the National Institute General Medical Sciences (NIGMS) Small Business Innovation Research (SBIR) grant (R43 GM130231) for the small animal studies and some of the material characterization in this work.

AUTHOR CONTRIBUTIONS

W.S., C.M., and C.L. designed the research; W.S., C.M., and C.L. performed material preparation and characterization; Q.L., J.L., X.Z., J.J., and D.L. conducted the *in vivo* pig studies; W.S., O.M., B.S.W. and E.B.R. conducted the *in vivo* rat studies; Q.L.,

W.S., C.M., and C.L. wrote the manuscript; Q.L., E.B.R., and D.L. revised the manuscript.

DECLARATION OF INTERESTS

W.S., C.M., and C.L. have a financial interest in Aleo BME. The other authors declare no competing interests.

Received: September 25, 2021
Revised: December 4, 2021
Accepted: December 25, 2021
Published: January 25, 2022

REFERENCES

1. Sharma, B., Fermanian, S., Gibson, M., Unterman, S., Herzka, D.A., Cascio, B., Coburn, J., Hui, A.Y., Marcus, N., Gold, G.E., and Elisseeff, J.H. (2013). Human cartilage repair with a photoreactive adhesive-hydrogel composite. Sci. Transl. Med. *5*, 167ra166.

2. Li, J., Celiz, A.D., Yang, J., Yang, Q., Wamala, I., Whyte, W., Seo, B.R., Vasilyev, N.V., Vlassak, J.J., Suo, Z., and Mooney, D.J. (2017). Tough adhesives for diverse wet surfaces. Science *357*, 378–381.

3. Singer, A.J., and Thode, H.C., Jr. (2004). A review of the literature on octylcyanoacrylate tissue adhesive. Am. J. Surg. *187*, 238–248.

4. Ma, C., Sun, J., Li, B., Feng, Y., Sun, Y., Xiang, L., Wu, B., Xiao, L., Liu, B., Petrovskii, V.S., et al. (2021). Ultra-strong bio-glue from genetically engineered polypeptides. Nat. Commun. *12*, 3613.

5. Sani, E.S., Kheirkhah, A., Rana, D., Sun, Z.M., Foulsham, W., Sheikhi, A., Khademhosseini, A., Dana, R., and Annabi, N. (2019). Sutureless repair of corneal injuries using naturally derived bioadhesive hydrogels. Sci Adv. *5*, eaav1281.

6. Guo, Y.C., Wang, Y., Zhao, X.H., Li, X., Wang, Q., Zhong, W., Mequanint, K., Zhan, R.X., Xing, M., and Luo, G.X. (2021). Snake extract-laden hemostatic bioadhesive gel cross-linked by visible light. Sci. Adv. *7*, eabf9635.

7. Sani, E.S., Lara, R.P., Aldawood, Z., Bassir, S.H., Nguyen, D., Kantarci, A., Intini, G., and Annabi, N. (2019). An antimicrobial dental light curable bioadhesive hydrogel for treatment of peri-implant diseases. Matter *1*, 926–944.

8. Annabi, N., Zhang, Y., Assmann, A., Sani, E.S., Vegh, A., Cheng, G., Dehghani, B., Ruiz-Esparza, G.U., Wang, X., Lassaletta, A.S., et al. (2017). Development of an elastic and adhesive sealant for surgical applications. Tissue Eng. A *23*, S123.

9. Bouten, P.J.M., Zonjee, M., Bender, J., Yauw, S.T.K., van Goor, H., van Hest, J.C.M., and Hoogenboom, R. (2014). The chemistry of tissue adhesive materials. Prog. Polym. Sci. *39*, 1375–1405.

10. Bhagat, V., and Becker, M.L. (2017). Degradable adhesives for surgery and tissue engineering. Biomacromolecules *18*, 3009–3039.

11. Zhao, Y.H., Wu, Y., Wang, L., Zhang, M.M., Chen, X., Liu, M.J., et al. (2017). Bio-inspired reversible underwater adhesive. Nat. Commun. *8*, 2218. https://doi.org/10.1038/s41467-017-02387-2.

12. Yang, Z., Ma, Z.W., Liu, S.Y., and Li, J.Y. (2021). Tissue adhesion with tough hydrogels: Experiments and modeling. Mech Mater *157*, 103800.

13. Fan, H.L., Wang, J.H., and Gong, J.P. (2021). Barnacle cement proteins-inspired tough hydrogels with robust, long-lasting, and repeatable underwater adhesion. Adv. Funct. Mater. *31*, 2009334.

14. Deng, J., Tang, Y.Y., Zhang, Q., Wang, C., Liao, M., Ji, P., Song, J.L., Luo, G.X., Chen, L., Ran, X.H., et al. (2019). A bioinspired medical adhesive derived from skin secretion of andrias davidianus for wound healing. Adv. Funct. Mater. *29*, 1809110.

15. von Byern, J., Grunwald, I., Kosok, M., Saporito, R.A., Dicke, U., Wetjen, O., Thiel, K., Borcherding, K., Kowalik, T., and Marchetti-Deschmann, M. (2017). Chemical characterization of the adhesive secretions of the salamander Plethodon shermani (Caudata, Plethodontidae). Sci. Rep. Uk *7*, 1.

16. Lee, B.P., Dalsin, J.L., and Messersmith, P.B. (2002). Synthesis and gelation of DOPA-modified poly(ethylene glycol) hydrogels. Biomacromolecules *3*, 1038–1047.

17. Yang, J.W., Bai, R.B., Chen, B.H., and Suo, Z.G. (2020). Hydrogel adhesion: a supramolecular synergy of chemistry, topology, and mechanics. Adv. Funct. Mater. *30*, 1901693.

18. Ma, Y.F., Ma, S.H., Wu, Y., Pei, X.W., Gorb, S.N., Wang, Z.K., Liu, W.M., and Zhou, F. (2018). Remote control over underwater dynamic attachment/detachment and locomotion. Adv. Mater. *30*, 1801595.

19. Maier, G.P., Rapp, M.V., Waite, J.H., Israelachvili, J.N., and Butler, A. (2015). Adaptive synergy between catechol and lysine promotes wet adhesion by surface salt displacement. Science *349*, 628–632.

20. Yuk, H., Varela, C.E., Nabzdyk, C.S., Mao, X.Y., Padera, R.F., Roche, E.T., and Zhao, X.H. (2019). Dry double-sided tape for adhesion of wet tissues and devices. Nature *575*, 169.

21. Guo, J., Kim, G.B., Shan, D., Kim, J.P., Hu, J., Wang, W., Hamad, F.G., Qian, G., Rizk, E.B., and Yang, J. (2017). Click chemistry improved wet adhesion strength of mussel-inspired citrate-based antimicrobial bioadhesives. Biomaterials *112*, 275–286.

22. Guo, J., Wang, W., Hu, J., Xie, D., Gerhard, E., Nisic, M., Shan, D., Qian, G., Zheng, S., and Yang, J. (2016). Synthesis and characterization of anti-bacterial and anti-fungal citrate-based mussel-inspired bioadhesives. Biomaterials *85*, 204–217.

23. Lu, X., Shi, S., Li, H., Gerhard, E., Lu, Z., Tan, X., Li, W., Rahn, K.M., Xie, D., Xu, G., et al. (2020). Magnesium oxide-crosslinked low-swelling citrate-based mussel-inspired tissue adhesives. Biomaterials *232*, 119719.

24. Guo, J., Sun, W., Kim, J.P., Lu, X., Li, Q., Lin, M., Mrowczynski, O., Rizk, E.B., Cheng, J., Qian, G., and Yang, J. (2018). Development of tannin-inspired antimicrobial bioadhesives. Acta Biomater. *72*, 35–44.

25. Huang, Y., Wang, Y., Tan, L., Sun, L., Petrosino, J., Cui, M.-Z., Hao, F., and Zhang, M. (2016). Nanospherical arabinogalactan proteins are a key component of the high-strength adhesive secreted by English ivy. Proc. Natl. Acad. Sci. U S A *113*, E3193–E3202.

26. Wong, V., Chan, K.W., and Kwan, A.K.H. (2013). Applying theories of particle packing and rheology to concrete for sustainable development. Organ Technol. Manage. Construct. An. Int. J. *5*, 844–851.

27. Wissinga, S.A., Kayserb, O., and Muller, R.H. (2004). Solid lipid nanoparticles for parenteral drug delivery. Adv. Drug Deliver. Rev. *56*, 1257–1272.

28. Rath, S.K., Ishack, A.M., Suryavansi, U.G., Chandrasekhar, L., and Patri, M. (2008). Phase morphology and surface properties of moisture cured polyurethane-urea (MCPU) coatings: Effect of catalysts. Prog. Org Coat *62*, 393–399.

29. Luo, N., Wang, D.N., and Ying, S.K. (1997). Hydrogen-bonding properties of segmented polyether poly(urethane urea) copolymer. Macromolecules *30*, 4405–4409.

30. Daniel-da-Silva, A.L., Moura Bordado, J.C., and Martin-Martinez, J.M. (2008). Moisture curing kinetics of isocyanate ended urethane quasi-

prepolymers monitored by IR Spectroscopy and DSC. J. Appl. Polym. Sci. *107*, 700–709.

31. Schon, P., Bagdi, K., Molnar, K., Markus, P., Pukanszky, B., and Vancso, G.J. (2011). Quantitative mapping of elastic moduli at the nanoscale in phase separated polyurethanes by AFM. Eur. Polym. J. *47*, 692–698.

32. Garcia, R. (2020). Nanomechanical mapping of soft materials with the atomic force microscope: methods, theory and applications. Chem. Soc. Rev. *49*, 5850–5884.

33. Dokukin, M.E., and Sokolov, I. (2012). Quantitative mapping of the elastic modulus of soft materials with HarmoniX and PeakForce QNM AFM modes. Langmuir *28*, 16060–16071.

34. Nishihira, S., and McCaffrey, T.V. (1988). The use of fibrin glue for the repair of experimental csf rhinorrhea. Laryngoscope *98*, 625–627.

35. Oh, J.W., Kim, S.H., and Whang, K. (2017). Traumatic cerebrospinal fluid leak: diagnosis and management. Korean J. Neurotrauma *13*, 63–67.

36. Esposito, F., Angileri, F.F., Kruse, P., Cavallo, L.M., Solari, D., Esposito, V., Tomasello, F., and Cappabianca, P. (2016). Fibrin sealants in dura sealing: a systematic literature review. PLoS One *11*, e0151533.

37. Kawai, H., Nakagawa, I., Nishimura, F., Motoyama, Y., Park, Y.-S., Nakamura, M., Nakase, H., Suzuki, S., and Ikada, Y. (2014). Usefulness of a new gelatin glue sealant system for dural closure in a rat durotomy model. Neurologia Medico-Chirurgica *54*, 640–646.

38. Reece, T.B., Maxey, T.S., and Kron, I.L. (2001). A prospectus on tissue adhesives. Am. J. Surg. *182*, 40S–44S.

39. Epstein, N.E. (2010). Dural repair with four spinal sealants: focused review of the manufacturers inserts and the current literature. Spine J. *10*, 1065–1068.

40. Zoia, C., Bongetta, D., Lombardi, F., Custodi, V.M., Pugliese, R., and Gaetani, P. (2015). First impressions about Adherus, a new dural sealant. J. Appl. Biomater. Funct. Mater. *13*, 372–375.

41. Annabi, N., Yue, K., Tamayol, A., and Khademhosseini, A. (2015). Elastic sealants for surgical applications. Eur. J. Pharmaceutics Biopharmaceutics *95*, 27–39.

42. Mehdizadeh, M., Weng, H., Gyawali, D., Tang, L., and Yang, J. (2012). Injectable citrate-based mussel-inspired tissue bioadhesives with high wet strength for sutureless wound closure. Biomaterials *33*, 7972–7983.

43. Mehdizadeh, M., and Yang, J. (2013). Design strategies and applications of tissue bioadhesives. Macromolecular Biosci *13*, 271–288.

44. Lee, G., Lee, C.K., and Bynevelt, M. (2010). DuraSeal-hematoma: concealed hematoma causing spinal cord compression. Spine (Phila Pa 1976) *35*, E1522–1524.

45. Bernal-Sprekelsen, M., Alobid, I., Mullol, J., Trobat, F., and Tomas-Barberan, M. (2005). Closure of cerebrospinal fluid leaks prevents ascending bacterial meningitis. Rhinology *43*, 277–281.

46. Preul, M.C., Campbell, P.K., Bichard, W.D., and Spetzler, R.F. (2007). Application of a hydrogel sealant improves watertight closures of duraplasty onlay grafts in a canine craniotomy model. J. Neurosurg. *107*, 642–650.

47. Rose, S., Prevoteau, A., Elziere, P., det, D., Marcellan, A., and Leibler, L. (2014). Nanoparticle solutions as adhesives for gels and biological tissues. Nature *505*, 382.

48. Tang, J.D., Li, J.Y., Vlassak, J.J., and Suo, Z.G. (2016). Adhesion between highly stretchable materials. Soft Matter. *12*, 1093–1099.

49. Kurokawa, T., Furukawa, H., Wang, W., Tanaka, Y., and Gong, J.P. (2010). Formation of a strong hydrogel-porous solid interface via the double-network principle. Acta Biomater. *6*, 1353–1359.

50. Cha, C.Y., Antoniadou, E., Lee, M., Jeong, J.H., Ahmed, W.W., Saif, T.A., Boppart, S.A., and Kong, H. (2013). Tailoring Hydrogel Adhesion to Polydimethylsiloxane Substrates Using Polysaccharide Glue. Angew Chem. Int. Ed. *52*, 6949–6952.

51. Roy, C.K., Guo, H.L., Sun, T.L., Bin Ihsan, A., Kurokawa, T., Takahata, M., et al. (2015). Self-Adjustable Adhesion of Polyampholyte Hydrogels. Adv. Mater. *27*, 7344–7348.

52. Yuk, H., Zhang, T., Parada, G.A., Liu, X.Y., and Zhao, X.H. (2016). Skin-inspired hydrogel-elastomer hybrids with robust interfaces and functional microstructures. Nat. Commun. *7*, 12028. https://doi.org/10.1038/ncomms12028.

53. Pawlicki, J.M., Pease, L.B., Pierce, C.M., Startz, T.P., Zhang, Y., and Smith, A.M. (2004). The effect of molluscan glue proteins on gel mechanics. J. Exp. Biol. *207*, 1127–1135.

54. Wilks, A.M., Rabice, S.R., Garbacz, H.S., Harro, C.C., and Smith, A.M. (2015). Double-network gels and the toughness of terrestrial slug glue. J. Exp. Biol. *218*, 3128–3137.

55. Rickett, T.A., Amoozgar, Z., Tuchek, C.A., Park, J., Yeo, Y., and Shi, R. (2011). Rapidly photo-cross-linkable chitosan hydrogel for peripheral neurosurgeries. Biomacromolecules *12*, 57–65.

56. Horio, T., Ishihara, M., Fujita, M., Kishimoto, S., Kanatani, Y., Ishizuka, T., Nogami, Y., Nakamura, S., Tanaka, Y., Morimoto, Y., and Maehara, T. (2010). Effect of photocrosslinkable chitosan hydrogel and its sponges to stop bleeding in a rat liver injury model. Artif Organs *34*, 342–347.

57. Mogal, V., Papper, V., Chaurasia, A., Feng, G., Marks, R., and Steele, T. (2014). Novel on-demand bioadhesion to soft tissue in wet environments. Macromol. Biosci. *14*, 478–484.

58. Elvin, C.M., Vuocolo, T., Brownlee, A.G., Sando, L., Huson, M.G., Liyou, N.E., Stockwell, P.R., Lyons, R.E., Kim, M., Edwards, G.A., et al. (2010). A highly elastic tissue sealant based on photopolymerised gelatin. Biomaterials *31*, 8323–8331.

59. International Commission on Non-Ionizing Radiation, P. (2004). Guidelines on limits of exposure to ultraviolet radiation of wavelengths between 180 nm and 400 nm (incoherent optical radiation). Health Phys. *87*, 171–186.

60. Melzer, B., Steinbrecher, T., Seidel, R., Kraft, O., Schwaiger, R., and Speck, T. (2010). The attachment strategy of English ivy: a complex mechanism acting on several hierarchical levels. J. R. Soc. Interf. *7*, 1383–1389.

61. Wang, N.G., Zhang, L.N., and Lu, Y.S. (2004). Effect of the particle size in dispersions on the properties of waterborne polyurethane/casein composites. Ind. Eng. Chem. Res. *43*, 3336–3342.

62. Maiti, R., Duan, M.Q., Danby, S.G., Lewis, R., Matcher, S.J., and Carre, M.J. (2020). Morphological parametric mapping of 21 skin sites throughout the body using optical coherence tomography. J. Mech. Behav. Biomed. *102*, 103501.

63. Strong, M.J., Carnahan, M.A., D'Alessio, K., Butlin, J.D.G., Butt, M.T., and Asher, A.L. (2015). Preclinical characterization and safety of a novel hydrogel for augmenting dural repair. Mater. Res. Express *2*, 095401.

64. Hafeman, A.E., Zienkiewicz, K.J., Zachman, A.L., Sung, H.J., Nanney, L.B., Davidson, J.M., and Guelcher, S.A. (2011). Characterization of the degradation mechanisms of lysine-derived aliphatic poly(ester urethane) scaffolds. Biomaterials *32*, 419–429.